Preprints (www.preprints.org) | NOT PEER-REVIEWED | Posted: 3 June 2019 doi:10.20944/preprints201906.0010.v1

Peer-reviewed version available at Sensors 2019, 19, 3459; doi:10.3390/s19163459

Article

Urban design factors influencing surface urban heat island in the humid subtropical region based on local climate zone

Yurong Shi [1], Yirui Xiang [1], Yufeng Zhang [1,*]

[1] State Key Laboratory of Subtropical Building Science, Department of Architecture, South China University of Technology, NO. 381 Wushan Road, Guangzhou 510640, China; arshiyurong@mail.scut.edu.cn (Y.S.)

* Correspondence: zhangyuf@scut.edu.cn; Tel.: +86-18664866529

Abstract: Surface urban heat island (SUHI) depicts the deteriorating thermal environment in high-density cities and local climate zone (LCZ) classification provides a universal protocol for SUHI identification. In this study, taking the central urbanized area of Guangzhou in the humid subtropical region of China as the study area, the maps or images of LCZ, land surface temperature (LST), SUHI and urban design factors were achieved by using Landsat satellite data, GIS database and a series of retrieval and classification algorithms, and the urban design factors influencing SUHI were investigated based on 625 samples of LCZs. The results show that in the summer daytime under the clear sky condition, the LST varied greatly from 26 °C to 40 °C and the SUHI changed in a wide range of -6 °C to 8 °C in the LCZs of the study area. Seven and five urban design factors influencing the summer daytime SUHI were identified for the two dominant LCZ of LCZs 1-5 (LCZ 1 to LCZ 5) and the mixed LCZ (containing at least three types of LCZs), respectively. The summer daytime SUHI prediction models were obtained by using the step-wise multiple linear regression, with the performance of R^2 of 0.697, RMSE of 1.21 °C, and the d value of 0.81 for the model of LCZs 1-5, and the values of 0.666, 1.66 °C, and 0.76 for the model of the mixed LCZ, indicating that the models can predict the changes of SUHI with LCZs to a large and satisfactory extent. This study presents a methodology to efficiently achieve a large sample of SUHI and urban design factors of LCZs in the largely urbanized cities, and provides information beneficial to the urban designs and regenerations in the humid subtropical region.

Keywords: Land surface temperature; Surface urban heat island, Local climate zone; Retrieval algorithms

1. Introduction

Land surface temperature (LST) is the primary important parameter to analyze urban climatology. It has a direct effect on the air temperature and mean radiant temperature which directly relate to the thermal environment. Thermal remote sensing of LST is a special case of observing LST which varies in response to the surface energy balance [1]. LST has been retrieved from remotely sensed thermal infrared (TIR) images, for instance, using a mono-window algorithm [2, 3], or a generalized single-channel method [4] for those of satellites with one TIR band.

The phenomenon that the air temperature in central urbanized areas is warmer than that of the surrounding non-urbanized areas called urban heat island (UHI). It is proportional to the degree of urbanization [5, 6] and closely related to urban climatology, thermal environment, and the quality of human life. UHI has been studied by in site measurement, remote sensing retrieval techniques, and

© 2019 by the author(s). Distributed under a Creative Commons CC BY license.

Preprints (www.preprints.org) | NOT PEER-REVIEWED | Posted: 3 June 2019 doi:10.20944/preprints201906.0010.v1

Peer-reviewed version available at Sensors 2019, 19, 3459; doi:10.3390/s19163459

modeling [7]. Thermal remote sensors observe the surface urban heat island (SUHI), or more specifically, they 'see' the spatial patterns of upwelling thermal radiance received by the remote sensors [1]. The advantage of remotely sensed SUHI is the indirect measurement in contrast to the direct in situ measurements of UHI, and it could also show the spatial variation with a broader region and a higher resolution.

As the traditional approach simply uses 'rural' and 'urban' to define UHI, with little attention to the diversity of the urban morphology, local climate zone (LCZ) [8] was proposed to accurately identify UHI. Primarily, researchers focus on two aspects of studies relating to the LCZ scheme. The first is the LCZ mapping study, for one city or a study area, taking LCZ as a lucid way to visualize urban morphology and using satellite images [9-11] or GIS data [12-14] to form LCZ maps. The second is the thermal properties of LCZs. For instance, Stewart et al. [15], Cardoso and Amorim [16], and Yang et al. [17] studied on the heat island magnitude ($\Delta T_{\mathrm{LCZ\ X\text{-}Y}}$) using screen-height temperature recorded by sensors installed in various LCZs. Leconte et al. [18], Kotharkar and Bagade [19], and Alexander and Mills [20] compared the air temperature variation in LCZs using mobile measurements. Geletič et al. [21], Cai et al. [10] and Bechtel et al. [22] adopted LST derived from remote sensor images to investigate the thermal environment difference of LCZs in one or multiple cities. Wang et al. [23] compared LST and LCZ changes for different years in Pearl River Delta (China). With the distinct definition of the urban landscape and classification hierarchy, LCZ is well-known as a good choice to UHI study. The above studies, however, mainly focused on the magnitude of UHI (SUHI) and thermal performance of LCZs, and very few on the main urban design factors influencing UHI (SUHI) in various LCZs.

Oke [5], Oke et al. [24], and Santamouris [6] have reviewed the urban design factors that have influences on UHI, including canyon radiative geometry, thermal properties of the material of building or vegetation, anthropogenic heat release, turbulent transfer, and so forth. Giridharan et al. [25, 26] established regression models with R^2 over 0.7 relating urban design variables of surface albedo, average height to floor area ratio, SVF, etc. with UHI. Jusuf and Wong [27] and Jusuf et al. [28] proposed empirical prediction models for an estate level air temperature in Singapore. The regression models were all built by using the data of field measurements, with many restrictions on sample size and spatial resolution. On the other hand, many of the urban design factors nowadays can be quickly and easily extracted based on remotely sensed retrieval algorithms [29-31] and Geographic Information System (GIS) techniques [32].

In the humid subtropical region of China, urban climate dramatically changed with the fast urbanization of the region, and the changes have significantly affected UHI intensity, building energy consumption, and people's living quality. The objective of this study is to identify the critical urban design factors that influence the SUHI intensity in the humid subtropical region based on a large sample of LCZs by using remotely sensed retrieval method and GIS techniques. Moreover, the SUHI prediction models will be proposed for LCZs in the humid subtropical region. The present study will provide a methodology to efficiently get the information of SUHI and the related urban design factors in cities in the largely urbanized zones, and the results are potentially beneficial to the urban designs and regenerations in the humid subtropical region.

Preprints (www.preprints.org) | NOT PEER-REVIEWED | Posted: 3 June 2019 doi:10.20944/preprints201906.0010.v1

Peer-reviewed version available at Sensors 2019, 19, 3459; doi:10.3390/s19163459

2. Materials and Methods

2.1 Study area and climate

Guangzhou, located at latitude 23°08′N and longitude 113°19′E, is a typical city in the humid subtropical region of China. The total population exceeded 14 million with a population density of 1883 people per km² at the end of 2016, based on data provided by the Statistical Bureau of Guangzhou (http://www.gzstats.gov.cn/). The center of Guangzhou, containing three districts of Tianhe, Yuexiu and Haizhu, is highly urbanized as Figure 1 shows. The central urbanized area of Guangzhou was selected as the study area, which was divided into 625 grids in 400 m×400 m according to the scale of LCZ (see red grids in Figure 1).

In Guangzhou, the long summer is hot and humid with abundant rainfall, and the winter is temperate and short. Guangzhou is in the monsoon region, with prevailing southeast winds in the summer and northern winds in the winter. According to the National Meteorological Information Center (http://data.cma.cn/) averages for over 30 years (from 1981 to 2010), the annual sunshine time is approximately from 1500 to 2000 h; the yearly rainfall is approximately 1801 mm; the monthly mean air temperature is 29.4 °C, and the relative humidity is 75% in July, and those values are 14.1 °C and 68%, respectively, in January in Guangzhou. Overheat is a big risk in summer, and the SUHI in the summer daytime is of great importance, especially under the clear sky condition.

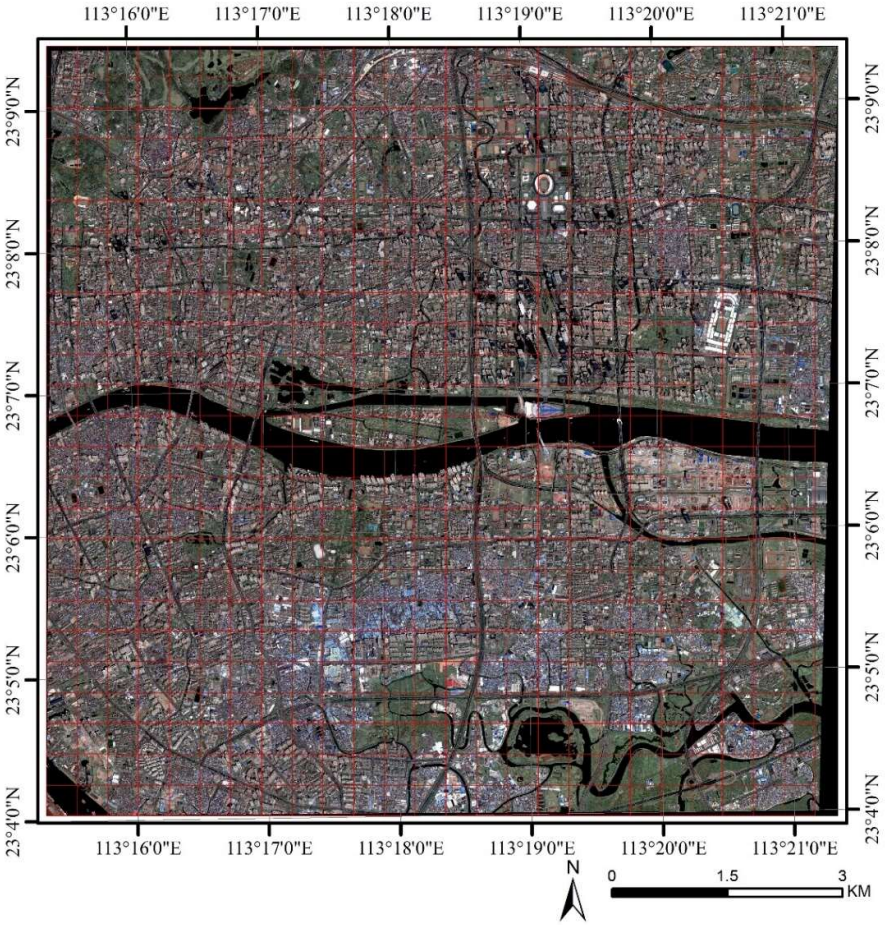

Figure 1. The visible image map with red grids of 400 m×400 m for the central urbanized area of Guangzhou. This image was obtained by the GeoEye-1 satellite on October 22nd, 2017.

Preprints (www.preprints.org) | NOT PEER-REVIEWED | Posted: 3 June 2019 doi:10.20944/preprints201906.0010.v1

Peer-reviewed version available at Sensors 2019, 19, 3459; doi:10.3390/s19163459

2.2 Local climate zone map

According to the LCZ concept by Stewart and Oke [8], the LCZ system consists of 17 standard LCZs, of which each LCZ has a characteristic urban form. Among the 17 LCZs, LCZs 1-10 are built-up areas with the difference in building density, height, or type, while LCZs A-G are land cover categories representing a distinct natural landscape. LCZ classification map was made for the central Guangzhou using the prevailing method of World Urban Database and Access Portal Tools (WUDAPT) from the website of http://www.wudapt.org/. There are more than 100 cities worldwide adopting WUDAPT to LCZ studies due to its' universal applicability. The procedure was quite lucid. Firstly, eight Landsat 8 images of Guangzhou (Table 1) that meet the criteria of cloudless were downloaded from the USGS website of https://earthexplorer.usgs.gov/. And then, these images were re-sampled from original 30 m resolution to 100 m resolution in the System for Automated Geoscientific Analyses (SAGA) software to fit the local scale. After that, the training areas of 12 types of LCZs (including 8 built-up LCZs and 4 land cover LCZs) in Guangzhou were digitized through Google Earth, and finally, based on the Landsat 8 images and the training samples, the random forest classifier was adopted to generate the LCZ map of Guangzhou in SAGA.

Each LCZ has a minimum radius of 200 m (i.e., a diameter of 400m) to match the local scale in urban climate study [8], and accordingly, the study area was divided into 625 grids in 400 m×400 m (Figure 1). The SUHI was calculated by the LST difference between a reference point and each LCZ. The mean LST value of LCZ D (LST D_{mean}) for the central urbanized Guangzhou was chosen as the LST of reference point because LCZ D represents a traditional non-urbanized area [15, 17]. The SUHI could accordingly be expressed as $\Delta T_{\text{LCZ X-D}}$, where X means either LCZ. A positive $\Delta T_{\text{LCZ X-D}}$ means urban heat island, and a negative $\Delta T_{\text{LCZ X-D}}$ means urban cool island.

Table 1 Landsat 8 images of Guangzhou for LCZ map

Entity ID	Date
LC81220442013333	2013/11/29
LC81220442013365	2013/12/31
LC81220442014288	2014/10/15
LC81220442015003	2015/01/03
LC81220442015019	2015/01/19
LC81220442015291	2015/10/18
LC81220442016038	2016/02/07
LC81220442016342	2016/12/07

2.3 Remotely sensed LST

The Landsat 8 satellite data was used for LST retrievals in this study. The image on the dates of September 18th, 2016 at Greenwich Mean Time (GMT) 2:51 am or the local time of 10:51 am was chosen, which is a recent summer daytime with the clear sky condition. There are two thermal infrared Bands for Landsat 8 TIRS (thermal infrared sensor). The Band 10 was used in this study, because the Band 11 showed the uncertainty of calibration by the USGS. The images from Landsat 8 OLI (Operational Land Imager) in the spatial resolution of 30 m and Landsat 8 TIRS in the spatial resolution of 100 m were obtained.

LST (T_s) was derived by using the improved mono-window algorithm [3] with the cloud-free pixels from the thermal infrared remote sensing data of Landsat satellite. The algorithm was based

Preprints (www.preprints.org) | NOT PEER-REVIEWED | Posted: 3 June 2019 doi:10.20944/preprints201906.0010.v1

Peer-reviewed version available at Sensors 2019, 19, 3459; doi:10.3390/s19163459

on the original mono-window algorithm [2], which had been verified as a reasonable LST estimation method by comparing with the simulated data or in situ measured data in the Israel–Egypt border [2] and Guangzhou [33]. The improved algorithm made development on the acquisition of estimate the parameter of effective mean atmospheric temperature, and showed a high accuracy of ~1.4 K for LST retrieval in various situations [3]. Ground emissivity (ε), effective mean atmospheric temperature (T_m) and atmospheric transmittance (τ) are the important input parameters for the algorithm as shown in Equations (1)-(3):

$$T_s=[a_{10}(1-C_{10}-D_{10})+[b_{10}(1-C_{10}-D_{10})+C_{10}+D_{10}]T_{10}-D_{10}T_m]/C_{10}, \quad (1)$$

$$C_{10}=\varepsilon\tau, \quad (2)$$

$$D_{10}=(1-\tau)[1+(1-\varepsilon)\tau], \quad (3)$$

where a_{10} and b_{10} are constants, a_{10} = −67.355351, b_{10} = 0.458606 for the temperature range of 0 to 50 °C; T_{10} is the brightness temperature in K.

Atmospheric transmittance is one of the most significant parameters for retrieving LST and is mainly affected by the water vapor content. The higher the water vapor content is, the lower the level of atmospheric transmittance. Wang et al. [3] proposed a method that uses the air humidity data from a nearby meteorological station to estimate water vapor content. The method was adopted to calculate the atmospheric transmittance, together with the empirical equation of tropical model proposed in Qin et al. [2].

2.4 Urban design factors

2.4.1 Choosing variables

There are a large number of urban design factors affecting SUHI. The present study took the nine variables into account, including surface albedo (α), sky view factor (SVF), vegetation cover ratio (λ_v), floor area ratio (FAR), building density (λ_b), ground emissivity (ε), complete surface area ratio (CSAR), mean building height (Z_h), and average height to building area ratio (HBDG). The detailed specifications on the variables are as follows.

Surface albedo is the ratio of upwelling irradiance from the surface that is illuminated by an unattenuated direct beam to the surface to downward irradiance, and is a critical parameter affecting the earth's climate and commonly required by global and regional climatic modeling and surface energy balance monitoring [34]. Given the solar elevation and azimuth angles, the thermal properties of land surface materials caused the changes in surface albedo, for instance, the canyon albedo can be increased and the near-ground air temperature can be decreased by increasing the surface albedo of walls [35].

SVF is a parameter that often used to describe the effect of building geometry on radiation exchange in the urban environment [36]. SVF is the ratio of the radiation received by a planar surface from the sky to that received from the entire hemispheric radiating environment [37]. A positive correlation between LST and SVF has been confirmed by [38, 39].

Vegetation cover ratio is an indispensability factor for analyzing the impact of vegetations on SUHI. Increasing the vegetation cover ratio is an efficient way to change the surrounding thermal environment. Vegetation cooled surrounding environments in the in the daytime of summer due to its shading and evaporation effects, while at night, the air temperature in tree shade was higher than that of the space without shade due to the block of upward long-wave radiation [40, 41].

Preprints (www.preprints.org) | NOT PEER-REVIEWED | Posted: 3 June 2019 doi:10.20944/preprints201906.0010.v1

Peer-reviewed version available at Sensors 2019, 19, 3459; doi:10.3390/s19163459

Floor area ratio and building density are the indices that urban planners and designers often used in their planning and design. Floor area ratio is the ratio of the whole floor area to the entire land area. Previous studies [35, 42] showed that, in the summer daytime conditions, the air temperature of urban canyon increased with the decreasing aspect ratio, because the heat gain increment of air was greater than thermal storage. As a smaller aspect ratio corresponds to a smaller floor area ratio, a negative relationship between the floor area ratio and UHI can be inferred. Building density is the ratio of gross building area to the entire land area. Bonafoni and Keeratikasikorn [43] shows the positive relationship between building density and LST or SUHI.

Ground emissivity is the ratio of energy emitted from land surface to that from an ideal blackbody at the same temperature. It affects LST or SUHI through long-wave radiations. It has not been reliably measured [44]. Wang et al. [3] got the average emissivity of representative terrestrial materials for Band 10 and Band 11 of Landsat 8 by using the ASTER spectral database [45], and the results showed that the emissivity of water, vegetation, soil, and building were 0.991, 0.973, 0.966, and 0.962, respectively.

The complete surface area proposed by Voogt and Oke [46] is the total sum roof, wall, and ground surface area. The larger the complete surface area is, the lower the SUHI or LST. The reason for this is similar to that of the impact of floor area ratio. The complete surface area ratio was used in the present study and refined as the ratio of the complete surface area to the entire land area.

Mean building height is an important parameter to calculate aerodynamic properties of urban areas, like zero-displacement length and roughness length [47]. Also, the average height to building area ratio is a good parameter represents the thermal mass of the environment with the effective distance [25, 27].

2.4.2 Urban design factors retrievals

1. Remotely sensed algorithms

Surface albedo was derived from Landsat satellite data. He et al. [29] proposed a unified direct estimation approach to evaluate surface albedo from Landsat MSS (Multi-Spectral Scanner), TM (Thematic Mapper), ETM+ (Enhanced Thematic Mapper Plus), and OLI data. This approach was adopted to obtain the surface albedo in the present study, as the validation results against ground measurements show that it was effective with a RMSE lower than 0.034.

The ground emissivity (ε_λ) in this study was the narrowband emissivity for the Band 10 and Band 11 of Landsat 8. It was retrieved by the widely used NDVI (Normalized Difference Vegetation Index) threshold method [30, 31]:

$$\varepsilon_\lambda = \begin{cases} \varepsilon_{s\lambda}, & NDVI < NDVI_s \\ \varepsilon_{v\lambda} P_v + \varepsilon_{s\lambda}(1-P_v) + C_\lambda, & NDVI_s \le NDVI \le NDVI_v \\ \varepsilon_{v\lambda} P_v + C_\lambda, & NDVI > NDVI_v \end{cases} \quad (4)$$

where the subscript s and v represent soil and vegetation pixels; $\varepsilon_{s\lambda}$ could be replaced by the emissivity of building $\varepsilon_{b\lambda}$ for an urban area, and the emissivity of vegetation and building for the Band 10 and Band 11 of Landsat 8 are shown in section 2.4.1; P_v is the vegetation cover ratio, and was retrieved by the dimidiate pixel model [48, 49]; C_λ is a term which takes into account the cavity effect due to surface roughness; $NDVI_s$ and $NDVI_v$ values were derived from the NDVI histogram [50].

Preprints (www.preprints.org) | NOT PEER-REVIEWED | Posted: 3 June 2019 doi:10.20944/preprints201906.0010.v1

Peer-reviewed version available at Sensors 2019, 19, 3459; doi:10.3390/s19163459

2. GIS database

Gál et al. [32] proposed two methods to computer continuous SVF values for a whole study area: vector based and raster based algorithms. The first algorithm was used in this study as the small SVF values can be included in the calculation of the cell average, whereas the latter algorithm has an overestimation on it [32]. The improvements by Gál and Unger [51] on tree-crown were also updated in the algorithm.

Design factors of vegetation area, building footprints, and heights were derived by the ArcGIS vectorization based on the high-resolution image (Figure 1) and the GIS database for the central urbanized area of Guangzhou. Based on these parameters, vegetation cover ratio, floor area ratio, building density, complete surface area ratio, and mean building height, and average height to building area ratio were calculated.

2.5 Data analysis and modelling

The data samples were obtained by combining the data from LCZ map, LST image and the urban design factors retrievals. They were saved into a database and put into SPSS statistics software for data analysis. The Pearson correlation analysis and the multiple linear regression were conducted on all data samples to observe the changing tendency of SUHI with various urban design factors, and to identify the key factors with significant and high correlations with SUHI. The five-sixth samples were then randomly selected for generating the SUHI prediction models by using the step-wise multiple linear regression method, and the remaining one-sixth samples were used to validate the models. The criteria of root mean square error (RMSE), index of agreement (d), and coefficient of determination (R^2) were chosen to reflect the performance of models. Figure 2 illustrates the details of data analysis framework in this study.

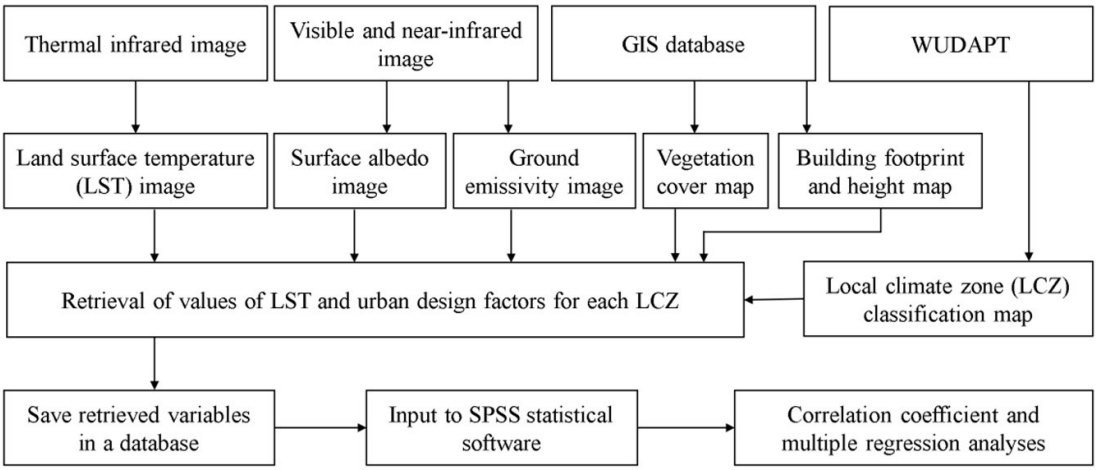

Figure 2. Framework of this study

Preprints (www.preprints.org) | NOT PEER-REVIEWED | Posted: 3 June 2019 doi:10.20944/preprints201906.0010.v1

Peer-reviewed version available at Sensors 2019, 19, 3459; doi:10.3390/s19163459

3. Results and discussion

3.1 LCZ classification map

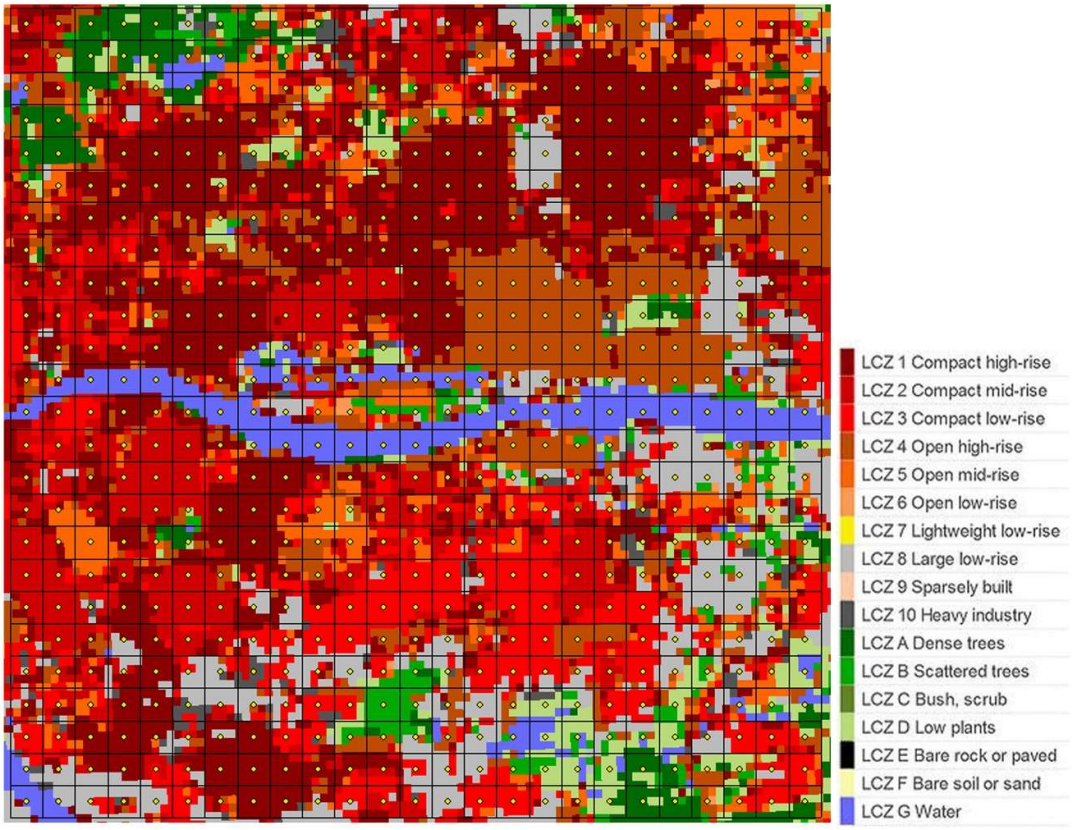

Figure 3. LCZ classification map with grids of 400 m×400 m for the central urbanized area of Guangzhou.

The LCZ classification map for the central urbanized area of Guangzhou is shown in Figure 3. It demonstrates that the central Guangzhou is a high-density heterogeneous area with 12 different LCZs. Totally 625 samples of LCZs were identified in the map. The proportion of various types of LCZs was analyzed as shown in Figure 4a. The mixed LCZ that contains at least three types of LCZs and not considered in the original paper of LCZ [8] accounts for the largest proportion of 43%. This is in accordance with many other metropolises in China, and the mixed LCZ was therefore treated as the first interest of this study. Besides, LCZ 1 to LCZ 5 (LCZs 1-5) that are built-up areas with open areas scattered sporadically account for a large proportion of 39%. LCZs 1-5 were then taken as the second interest of this study. The detailed proportion of each LCZ in LCZs 1-5 was further investigated as shown in Figure 4b, indicating that LCZ 1 takes the largest part, followed by the mix of any two types and LCZs 2-4.

Preprints (www.preprints.org) | NOT PEER-REVIEWED | Posted: 3 June 2019 doi:10.20944/preprints201906.0010.v1

Peer-reviewed version available at Sensors 2019, 19, 3459; doi:10.3390/s19163459

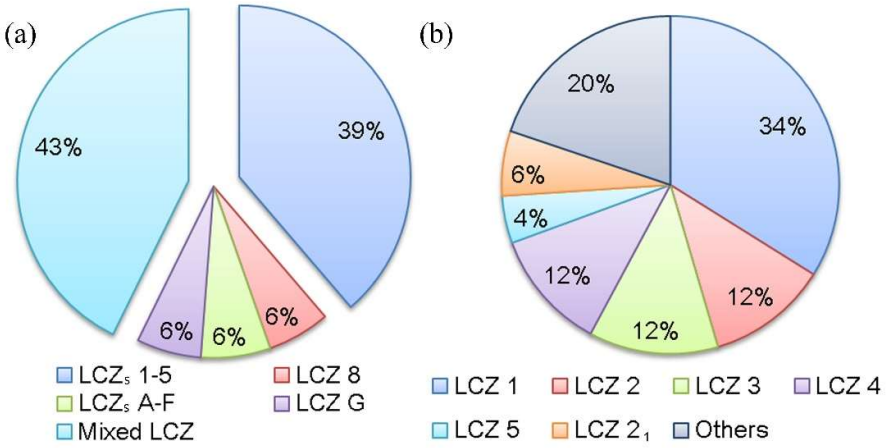

Figure 4. The proportion of (**a**) the whole LCZ classification, and (**b**) the built-up LCZs from LCZ 1 to LCZ 5 for the central urbanized area of Guangzhou. "Others" means containing any two types of LCZs 1-5.

3.2 Retrievals of LST and urban design factors

The retrieved images for LST, SVF, surface albedo and ground emissivity are shown in Figure 5. The 3D map for land surface cover is shown in Figure 6.

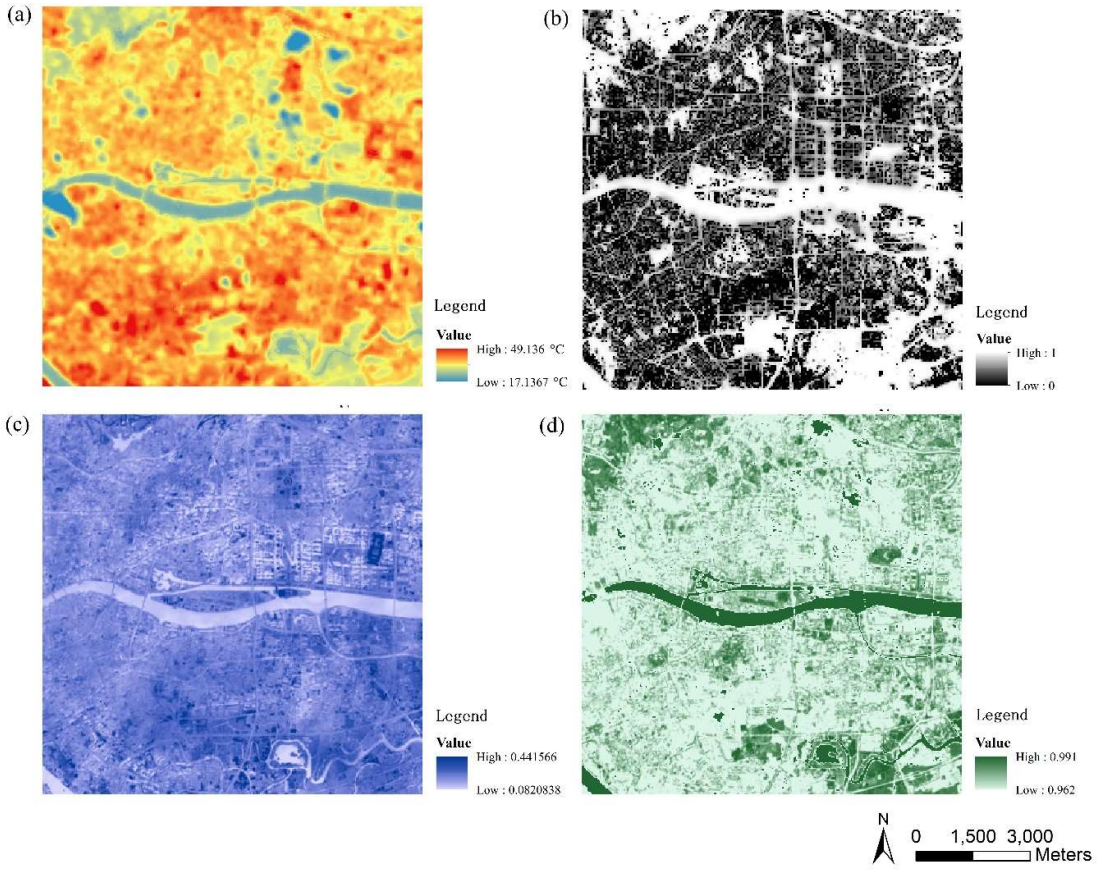

Figure 5. (a) LST, (b) sky view factor, (c) surface albedo, and (b) ground emissivity retrieval images for the central urbanized area of Guangzhou.

Preprints (www.preprints.org) | NOT PEER-REVIEWED | Posted: 3 June 2019 doi:10.20944/preprints201906.0010.v1

Peer-reviewed version available at Sensors 2019, 19, 3459; doi:10.3390/s19163459

Figure 6. 3D Land surface cover map for the central urbanized area of Guangzhou.

Combining Figures 3, 5, and 6, the medians and variations of LST, SUHI, and urban design factors for each LCZ in the central Guangzhou were obtained as shown in Figure 7. Ten types of LCZ, including 6 built-up LCZs, 3 natural land cover LCZs and one mixed LCZ, are presented, as the samples for other types are quite small.

Preprints (www.preprints.org) | NOT PEER-REVIEWED | Posted: 3 June 2019 doi:10.20944/preprints201906.0010.v1

Peer-reviewed version available at Sensors 2019, 19, 3459; doi:10.3390/s19163459

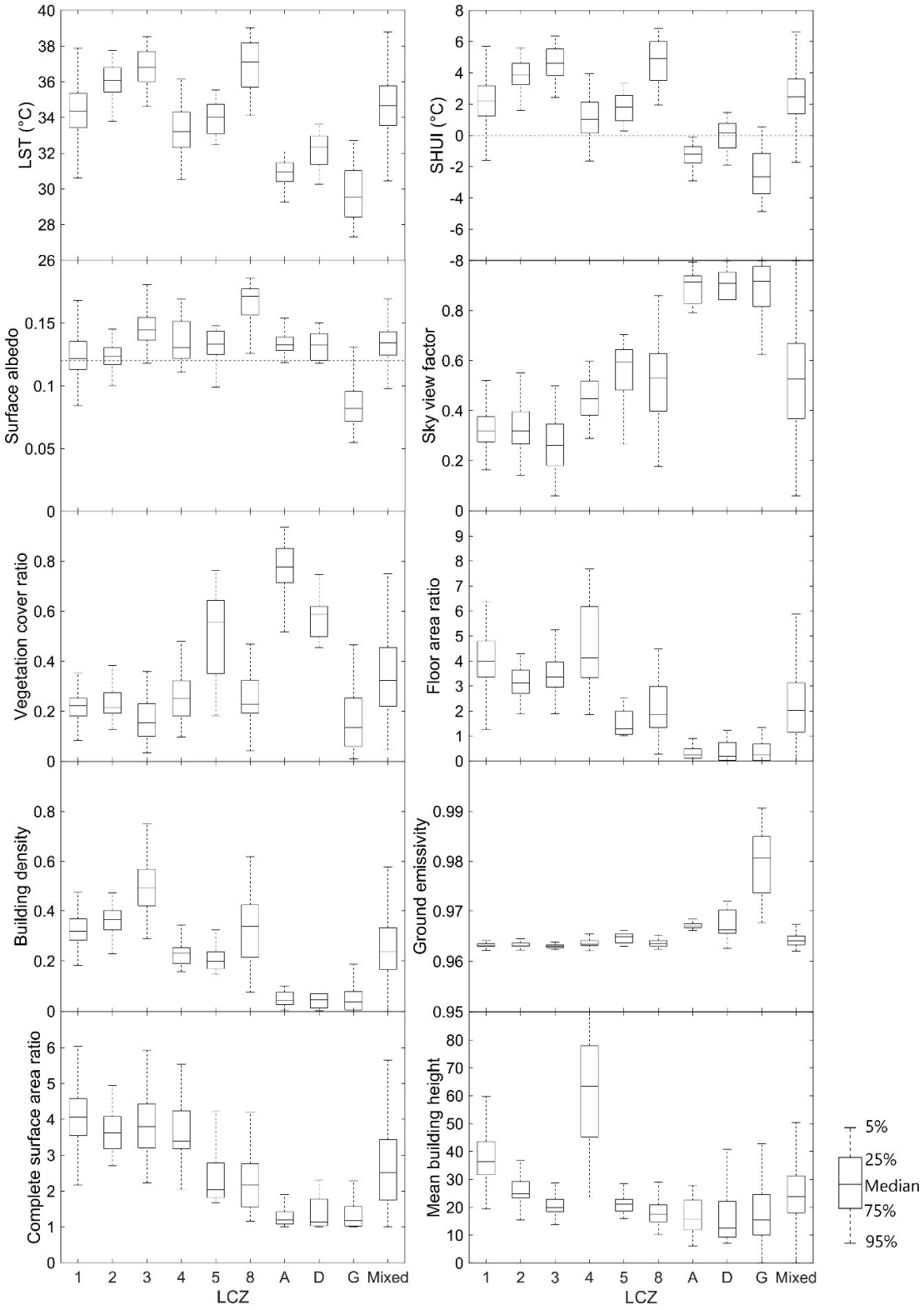

Figure 7. Box plots of LST, SUHI and urban design factors for the LCZs in central urbanized area of Guangzhou.

In the summer daytime under the clear sky condition, the LST vaired greatly from 26 °C to 40 °C, and the SUHI changed in a wide range of -6 °C to 8 °C in the LCZs of the study area. The LST and SUHI in variuous LCZs are quite similar with the findings by Bechtel et al. [22] on a comparison of

Preprints (www.preprints.org) | NOT PEER-REVIEWED | Posted: 3 June 2019 doi:10.20944/preprints201906.0010.v1

Peer-reviewed version available at Sensors 2019, 19, 3459; doi:10.3390/s19163459

50 cities, showing the orders from high to low as LCZ 3 > LCZ 2 > LCZ 1, LCZ 8 > LCZ 5 > LCZ 4, and LCZ D > LCZ A > LCZ G. The mixed LCZ showed the median between that of the built-up and natural LCZs and the largest variation. The surface albedo varied in the range of 0.05 to 0.2. It increased when the built-up areas became more open or the buildings became lower, and it was quite similar for the green natural areas of trees (LCZ A) and plants (LCZ D), while that of water (LCZ G) was much lower. The sky view factor changed greatly from 0 to 1. It was larger in the natural and open built-up areas, and again, the mixed LCZ showed a large variation range due to its complexity. The vegetation cover ratio nearly kept the same level of 0.2 for the build-up areas except LCZ 5, and there is no doubt that LCZ A (Dense trees) had the largest values. The two areas of LCZ 1 and 4 with high-rise buildings showed higher floor area ratios (~4), and the two areas of LCZ 3 and 8 with low-rise buildings showed larger building densities (0.5 and 0.3), while the mixed LCZ showed the lower medians of floor area ratio (2) and building density (0.2) with larger variations. The ground emissivity was very much similar for all build-up areas (~0.96), and that of water (0.98) was higher than that of trees and low plants (0.965). The complete surface area ratio varied from 1 to 6, and decreased when the built-up areas became more open or the buildings became lower. The mean building height was largest in LCZ 4, because the Central Business District (CBD) in Guangzhou with many super high-rise buildings was involved in this type of LCZ.

3.3 The correlations between urban design factors and SUHI

Since the multiple linear regression showed that the average height to building area ratio had a collinearity with the mean building height, the factor of the average height to building area ratio was removed and the remaining eight factors of surface albedo, sky view factor, vegetation cover ratio, floor area ratio, building density, ground emissivity, complete surface area ratio, and mean building height were assumed to play roles in determining SUHI.

In the present study, 228 data samples were obtained for LCZs 1-5 and 261 data samples were obtained for the mixed LCZ. LCZs 1-5 were regular built-up areas with various urban design factors, and it would provide useful information for design of urban built-up areas by polling all LCZs 1-5 into a data group for analysis. On the other hand, the mixed LCZ were quite complicated and could not be simply treated as built-up or natural land areas. And therefore, the mixed LCZ was treated as another group of data for analysis.

3.3.1 Pearson correlation analysis

The Pearson correlation analysis results for LCZs 1-5 are shown in Figure 8. The factors of surface albedo and building density showed positive correlations with the summer daytime SUHI, while other factors showed negative correlations. The changing tendencies of the factors of vegetation cover ratio, floor area ratio, building density, ground emissivity, mean building height and complete surface area ratio are in good agreement with the previous findings in section 2.4.1. The correlation in its absolute value was larger for building density and mean building height, followed by the factors of floor area ratio and sky view factor, while less than 0.3 for others.

Preprints (www.preprints.org) | NOT PEER-REVIEWED | Posted: 3 June 2019 doi:10.20944/preprints201906.0010.v1

Peer-reviewed version available at Sensors 2019, 19, 3459; doi:10.3390/s19163459

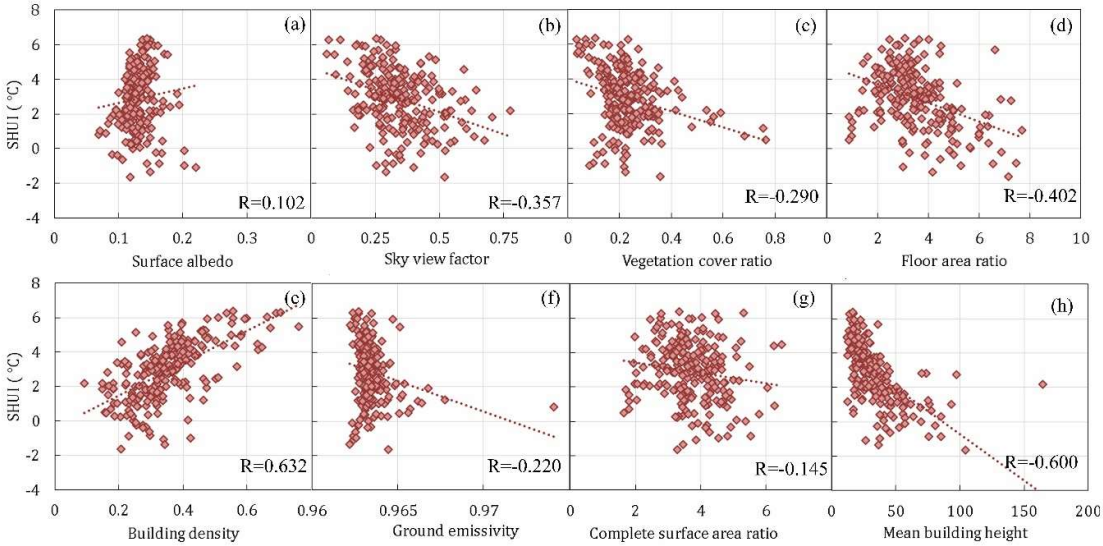

Figure 8. SUHI vs urban design factors of (a) surface albedo, (b) sky view factor, (c) vegetation cover ratio, (d) floor area ratio, (e) building density, (f) ground emissivity, and (g) complete surface area ratio, and (h) mean building height for LCZs 1-5 in central urbanized area of Guangzhou.

The Pearson correlation analysis results for the mixed LCZ are shown in Figure 9. The factors of surface albedo, floor area ratio, building density and complete surface area ratio showed positive correlations with the summer daytime SUHI, while other factors showed negative correlations. The changing tendencies of vegetation cover ratio, building density, ground emissivity and mean building height are in good agreement with LCZs 1-5 and the previous findings. The correlation in its absolute value was larger for building density and ground emissivity, followed by the factors of sky view factor and vegetation cover ratio, while less than 0.4 for others.

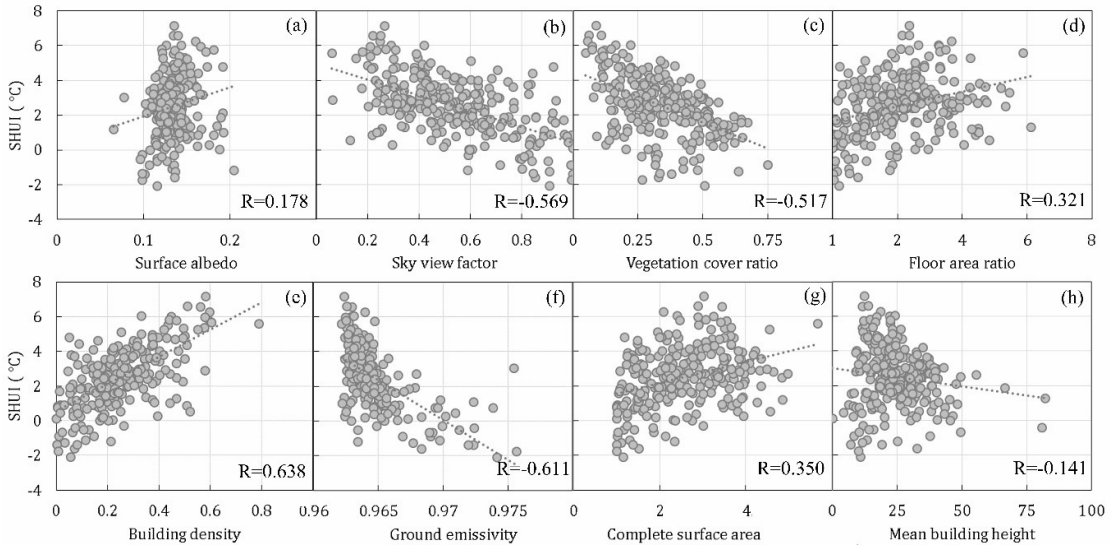

Figure 9. SUHI vs urban design factors of (a) surface albedo, (b) sky view factor, (c) vegetation cover ratio, (d) floor area ratio, (e) building density, (f) ground emissivity, and (g) complete surface area ratio, and (h) mean building height for the mixed LCZ in central urbanized area of Guangzhou.

Preprints (www.preprints.org) | NOT PEER-REVIEWED | Posted: 3 June 2019 doi:10.20944/preprints201906.0010.v1

Peer-reviewed version available at Sensors 2019, 19, 3459; doi:10.3390/s19163459

Both for LCZs 1-5 and the mixed LCZ, the correlations of surface albedo and sky view factor with the summer daytime SUHI showed opposite signs to those of previous findings. Furthermore, the two factors of floor area ratio and complete surface area ratio showed opposite correlations in LCZs 1-5 and in the mixed LCZ. The above abnormal results indicate that the Pearson correlation analysis may not reveal the actual correlations in the case of multivariate changes.

3.3.2 Partial correlation analysis

The multiple regression results for LCZs 1-5 and the mixed LCZ are presented in Table 2. The results of Pearson correlation analysis are shown together for comparison.

Table 2. The Pearson correlation and multiple regression results of SUHI vs urban design factors

Variables	LCZs 1-5					Mixed LCZ				
	Coefficient				Sig.	Coefficient				Sig.
	B	β	Pearson correlation	Partial correlation		B	β	Pearson correlation	Partial correlation	
Constant	*156.351*				*.041*	*436.730*				*.000*
α	*-17.725*	*-.218*	*.102*	*-.293*	*.000*	*-14.348*	*-.154*	*.178*	*-.212*	*.001*
SVF	*4.450*	*.316*	*-.357*	*.218*	*.001*	*EX*	*EX*	*EX*	*EX*	*EX*
λ_v	*-5.088*	*-.326*	*-.290*	*-.312*	*.000*	*-3.836*	*-.333*	*-.517*	*-.372*	*.000*
FAR	*-.477*	*-.366*	*-.402*	*-.384*	*.000*	*EX*	*EX*	*EX*	*EX*	*EX*
λ_b	*11.846*	*.798*	*.632*	*.516*	*.000*	*7.209*	*.588*	*.638*	*.471*	*.000*
ε	*-158.179*	*-.097*	*-.220*	*-.133*	*.047*	*-445.594*	*-.594*	*-.611*	*-.564*	*.000*
CSAR	*-.429*	*-.223*	*-.145*	*-.232*	*.000*	*-1.155*	*-.660*	*.350*	*-.520*	*.000*
R^2	*0. 665*					*0.652*				
F	*62.613*					*95.799*				
Number	*228*					*261*				

B = unstandardized coefficient. β = standardized coefficient, Sig. = Significant level, EX = regression model excluded the variable.

In LCZs 1-5, the factors of sky view factor and building density showed positive partial correlations with the summer daytime SUHI, while other factors showed negative partial correlations. Compared to those of Pearson correlation, it can be known that the partial correlations became opposite for the factors of surface albedo and sky view factor. In the mixed LCZ, the factors of building density showed positive partial correlations with the summer daytime SUHI, while other factors showed negative or insignificant partial correlations. The partial correlations were opposite to the Pearson correlations for the factors of surface albedo and complete surface area ratio.

Compared with the specifications in section 2.4.1, it can be found that all the results of partial correlations are in good agreement with the well-known facts or previous findings, indicating that the partial correlation is more suitable to capturing the actual correlations in the case of multivariate changes. The exclusion of mean building height and average height to building area ratio in the regressions both for LCZs 1-5 and the mixed LCZ was due to their significant levels (P) larger than 0.05. In addition, since floor area ratio and sky view factor had collinearities with building density in the mixed LCZ, both of them were removed from the regression.

3.4 The SUHI prediction models and their validations

3.4.1 The SUHI prediction models

The randomly selected five-sixth samples were used for generating the summer daytime SUHI prediction models by using step-wise multiple linear regression method, in which the factors with

Preprints (www.preprints.org) | NOT PEER-REVIEWED | Posted: 3 June 2019 doi:10.20944/preprints201906.0010.v1

Peer-reviewed version available at Sensors 2019, 19, 3459; doi:10.3390/s19163459

an insignificant impact (P>0.05) or with the collinearity problem were removed. Finally, seven factors for LCZs 1-5, and five factors for the mixed LCZ were determined, as shown in Table 3.

Table 3. The step-wise multiple regression results of SUHI prediction model

Variables	LCZs 1-5				Mixed LCZ			
	Coefficient			Sig.	Coefficient			Sig.
	B	β	Partial correlation		B	β	Partial correlation	
Constant	*190.139*			*.012*	*458.821*			*.000*
α	*-22.816*	*-.277*	*-.377*	*.000*	*-10.958*	*-.119*	*-.168*	*.014*
SVF	*4.952*	*.349*	*.249*	*.001*	*EX*	*EX*	*EX*	*EX*
λ_v	*-5.607*	*-.346*	*-.343*	*.000*	*-3.768*	*-.325*	*-.376*	*.000*
FAR	*-.459*	*-.342*	*-.363*	*.000*	*EX*	*EX*	*EX*	*EX*
λ_b	*12.241*	*.844*	*.541*	*.000*	*6.465*	*.538*	*.445*	*.000*
ε	*-192.805*	*-.124*	*-.180*	*.014*	*-468.869*	*-.623*	*-.595*	*.000*
CSAR	*-.436*	*-.233*	*-.256*	*.000*	*-1.128*	*-.646*	*-.521*	*.000*
R^2	*0.697*				*.666*			
F	*60.058*				*84.616*			
Number	*190*				*217*			

B = unstandardized coefficient, β = standardized coefficient, Sig. = Significant level, EX = regression model excluded the variable.

According to Table 3, the summer daytime SUHI prediction model for the LCZs 1-5 in the humid subtropical region was obtained as:

$$SUHI = 190.139 - 22.816\alpha + 4.952SVF - 5.607\lambda_v - 0.459FAR + 12.241\lambda_b - 192.805\varepsilon - 0.436CSAR, \quad R^2 = 0.697 \tag{5}$$

and accordingly, the summer daytime LST prediction model was obtained as:

$$LST = LST\ D_{mean} + 190.139 - 22.816\alpha + 4.952SVF - 5.607\lambda_v - 0.459FAR + 12.241\lambda_b - 192.805\varepsilon - 0.436CSAR, \quad R^2 = 0.697 \tag{6}$$

The summer daytime SUHI and LST prediction models for the mixed LCZ in the humid subtropical region were obtained as:

$$SUHI = 458.821 - 10.958\alpha - 3.768\lambda_v + 6.465_{\lambda_b} - 468.869\varepsilon - 0.646CSAR, \ R^2 = 0.666 \tag{7}$$

$$LST = LST\ D_{mean} + 458.821 - 10.958\alpha - 3.768\lambda_v + 6.465\lambda_b - 468.869\varepsilon - 0.646CSAR, \ R^2 = 0.666 \tag{8}$$

3.4.2 Validations

The comparisons between the observed and the predicted SUHI values for the remaining one-sixth samples of LCZs 1-5 and the mixed LCZ are illuminated in Figure 10. The observed and predicted values had a positive correlation, with R^2 of 0.478 and 0.554 for the models of LCZs 1-5 and the mixed LCZ, respectively. The RMSE values were obtained as 1.21°C and 1.66°C for the LCZs 1-5 and mixed LCZ models, respectively, showing a barely satisfactory performance. A value of d close to 1.0 indicates that the model prediction approaches the observed variable. The d values of the LCZs 1-5 and mixed LCZ models were determined to be 0.81 and 0.76, respectively, indicating that the prediction models could predict the changes of SUHI with LCZs to a large extent.

Preprints (www.preprints.org) | NOT PEER-REVIEWED | Posted: 3 June 2019 doi:10.20944/preprints201906.0010.v1

Peer-reviewed version available at Sensors 2019, 19, 3459; doi:10.3390/s19163459

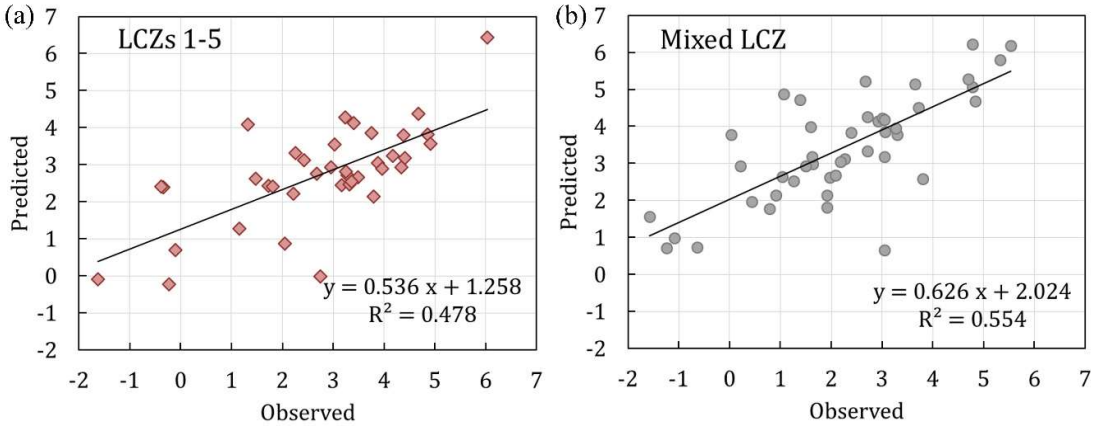

Figure 10. Observed vs Predicted SUHI values for (a) LCZs 1-5 and (b) the mixed LCZ models. The linear regression with solid lines are shown.

4. Conclusions

In the present study, taking the central urbanized area of Guangzhou in the humid subtropical region of China as the study area, the maps or images of LCZ, LST, SUHI and urban design factors were achieved by using Landsat satellite data, GIS database and a series of retrieval and classification algorithms, and the urban design factors influencing the summer daytime SUHI were investigated based on a large sample (625 samples) of LCZs. The main conclusions are as follows.

The central urbanized area of Guangzhou is a high-density heterogeneous area with 12 different LCZs, in which the mixed LCZ that contains at least three types of LCZs and the built-up LCZs 1-5 are dominant.

In the summer daytime under the clear sky condition, the LST varied greatly from 26 °C to 40 °C and the SUHI changed in a wide range of -6 °C to 8 °C in the LCZs of the study area. For the built-up LCZs, the LST or SUHI became higher when the buildings became lower, together with higher surface albedo and building density and lower floor area ratio and complete surface area ratio; and the LST or SUHI became lower when the area became more open, together with higher surface albedo, SVF and vegetation cover ratio, and lower floor are ratio, building density and complete surface area ratio.

Seven urban design factors influencing the summer daytime SUHI were identified for LCZs 1-5, in which sky view factor and building density showed positive partial correlations, while the factors of surface albedo, vegetation cover ratio, floor area ratio, ground emissivity, and complete surface area ratio showed negative partial correlations.

Five urban design factors influencing the summer daytime SUHI were identified for the mixed LCZ, in which building density showed positive partial correlations, while the factors of surface albedo, vegetation cover ratio, ground emissivity, and complete surface area ratio showed negative partial correlations.

The summer daytime SUHI prediction models were obtained by using the step-wise multiple linear regression, showing the performance of R^2 of 0.697, RMSE of 1.21 °C, and the d value of 0.81 for the model of LCZs 1-5, and the values of 0.666, 1.66 °C, and 0.76 for the model of the mixed LCZ, respectively. It is concluded that the prediction models can predict the changes of SUHI with LCZs to a large and satisfactory extent.

Limitations and prospects are briefly listed below. Only one thermal infrared image in the summer daytime was used in this study. It can provide more useful information by including more images, especially those in the summer nighttime and other seasons, and this study provides an efficient and feasible methodology for doing that. The retrieval of air temperature has been studied by many researchers and several algorithms have been proposed. The urban canopy air temperature and its related UHI are recommended to be studied. Although the multiple linear prediction models

Preprints (www.preprints.org) | NOT PEER-REVIEWED | Posted: 3 June 2019 doi:10.20944/preprints201906.0010.v1

Peer-reviewed version available at Sensors 2019, 19, 3459; doi:10.3390/s19163459

are effective and simple to use, especially for the early stage of urban planning and design, the following work is worth doing to improve the model's performance: 1) to include more potential factors, for instance, the population scale and related anthropogenic heat; 2) to re-construct the urban design factors into indicators by following a clear physical mechanism; and 3) to consider the interactions of neighboring LCZs.

Author Contributions: Conceptualization, Y.S. and Y.Z.; data curation, Y.S. and Y.X.; formal analysis, Y.S.; funding acquisition, Y.Z.; Investigation, Y.S. and Y.X.; Methodology, Y.S. and Y.Z.; project administration, Y.Z; supervision, Y.Z.; validation, Y.S.; visualization, Y.S.; writing—original draft, Y.S. and Y.X.; writing—review and editing, Y.Z. and Y.S..

Funding: This research was funded by National Natural Science Foundation of China, grant number 51578243.

Conflicts of Interest: The authors declare no conflict of interest.

References

1. Voogt JA,Oke TR. Thermal remote sensing of urban climates. *Remote Sensing of Environment* **2003**, *86*, 370-384. Available online: http://dx.doi.org/10.1016/S0034-4257(03)00079-8.
2. Qin Z, Karnieli A,Berliner P. A mono-window algorithm for retrieving land surface temperature from Landsat TM data and its application to the Israel-Egypt border region. *International Journal of Remote Sensing* **2001**, *22*, 3719-3746. Available online: http://dx.doi.org/10.1080/01431160010006971.
3. Wang F, Qin Z, Song C, Tu L, Karnieli A,Zhao S. An improved Mono-window algorithm for land surface temperature retrieval from Landsat 8 Thermal Infrared Sensor data. *Remote Sensing* **2015**, *7*, 4268-4289. Available online: http://dx.doi.org/10.3390/rs70404268.
4. Jiménez-Muñoz JC,Sobrino JA. A generalized single-channel method for retrieving land surface temperature from remote sensing data. *Journal of Geophysical Research Atmospheres* **2003**, *108*, 1-9. Available online: http://dx.doi.org/10.1029/2003JD003480.
5. Oke TR. *Boundary layer climates*. Second edition ed. Routledge: London, 1987.
6. Santamouris M. *Energy and climate in the urban built environment*. James & James: UK, 2001.
7. Lu D,Weng Q. Spectral mixture analysis of ASTER images for examining the relationship between urban thermal features and biophysical descriptors in Indianapolis, Indiana, USA. *Remote Sensing of Environment* **2006**, *104*, 157-167. Available online: http://dx.doi.org/10.1016/j.rse.2005.11.015.
8. Stewart ID,Oke TR. Local climate zones for urban temperature studies. *Bull. Amer. Meteor. Soc.* **2012**, *93*, 1879-1900. Available online: http://dx.doi.org/10.1175/BAMS-D-11-00019.1.
9. Danylo O, See L, Bechtel B, Schepaschenko D,Fritz S. Contributing to WUDAPT: A Local Climate Zone Classification of Two Cities in Ukraine. *IEEE Journal of Selected Topics in Applied Earth Observations and Remote Sensing* **2016**, *9*, 1841-1853. Available online: http://dx.doi.org/10.1109/JSTARS.2016.2539977.
10. Cai M, Ren C, Xu Y, Lau KK-L,Wang R. Investigating the relationship between local climate zone and land surface temperature using an improved WUDAPT methodology – A case study of Yangtze River Delta, China. *Urban Climate* **2018**, *24*, 485-502. Available online: http://dx.doi.org/10.1016/j.uclim.2017.05.010.
11. Verdonck M-L, Okujeni A, van der Linden S, Demuzere M, De Wulf R,Van Coillie F. Influence of neighbourhood information on 'Local Climate Zone' mapping in heterogeneous cities. *International Journal of Applied Earth Observation and Geoinformation* **2017**, *62*, 102-113. Available online: http://dx.doi.org/10.1016/j.jag.2017.05.017.

Preprints (www.preprints.org) | NOT PEER-REVIEWED | Posted: 3 June 2019 doi:10.20944/preprints201906.0010.v1

Peer-reviewed version available at Sensors 2019, 19, 3459; doi:10.3390/s19163459

12. Zheng Y, Ren C, Xu Y, Wang R, Ho J, Lau K,Ng E. GIS-based mapping of Local Climate Zone in the high-density city of Hong Kong. *Urban Climate* **2018**, *24*, 419-448. Available online: http://dx.doi.org/10.1016/j.uclim.2017.05.008.

13. Geletič J,Lehnert M. GIS-based delineation of local climate zones: The case of medium-sized Central European cities. **2016**, *24*, 2. Available online: http://dx.doi.org/10.1515/mgr-2016-0012.

14. Mitraka Z, Frate FD, Chrysoulakis N,Gastellu-Etchegorry J. Exploiting Earth Observation data products for mapping Local Climate Zones. Joint Urban Remote Sensing Event (JURSE). Lausanne, Switzerland, 30 March-1 April; 2015.

15. Stewart ID, Oke TR,Krayenhoff ES. Evaluation of the 'local climate zone' scheme using temperature observations and model simulations. *Int. J. Climatol.* **2014**, *34*, 1062-1080. Available online: http://dx.doi.org/10.1002/joc.3746.

16. Cardoso RS,Amorim M. Urban heat island analysis using the 'local climate zone' scheme in Presidente Prudente, Brazil. **2018**, Available online: http://dx.doi.org/10.14198/INGEO2018.69.07.

17. Yang X, Yao L, Jin T, Peng LLH, Jiang Z, Hu Z,Ye Y. Assessing the thermal behavior of different local climate zones in the Nanjing metropolis, China. *Building and Environment* **2018**, *137*, 171-184. Available online: http://dx.doi.org/10.1016/j.buildenv.2018.04.009.

18. Leconte F, Bouyer J, Claverie R,Pétrissans M. Estimation of spatial air temperature distribution at sub-mesoclimatic scale using the LCZ scheme and mobile measurements. 9th International Conference on Urban Climate. Toulouse, France, 2015.

19. Kotharkar R,Bagade A. Evaluating urban heat island in the critical local climate zones of an Indian city. *Landscape and Urban Planning* **2018**, *169*, 92-104. Available online: http://dx.doi.org/10.1016/j.landurbplan.2017.08.009.

20. Alexander P,Mills G. Local Climate Classification and Dublin's Urban Heat Island. *Atmosphere* **2014**, *5*, 755-774. Available online: http://dx.doi.org/10.3390/atmos5040755.

21. Geletič J, Lehnert M,Dobrovolný P. Land Surface Temperature Differences within Local Climate Zones, Based on Two Central European Cities. *Remote Sensing* **2016**, *8*, 788. Available online: http://dx.doi.org/10.3390/rs8100788.

22. Bechtel B, Demuzere M, Mills G, Zhan W, Sismanidis P, Small C,Voogt J. SUHI analysis using Local Climate Zones—A comparison of 50 cities. *Urban Climate* **2019**, *28*, 100451. Available online: http://dx.doi.org/10.1016/j.uclim.2019.01.005.

23. Wang R, Cai M, Ren C, Bechtel B, Xu Y,Ng E. Detecting multi-temporal land cover change and land surface temperature in Pearl River Delta by adopting local climate zone. *Urban Climate* **2019**, *28*, 100455. Available online: http://dx.doi.org/10.1016/j.uclim.2019.100455.

24. Oke TR, Johnson GT, Steyn DG,Watson ID. Simulation of surface urban heat islands under 'ideal' conditions at night part 2: Diagnosis of causation. *Bound-Layer Meteor.* **1991**, *56*, 339-358. Available online: http://dx.doi.org/10.1007/bf00119211.

25. Giridharan R, Lau SSY, Ganesan S,Givoni B. Urban design factors influencing heat island intensity in high-rise high-density environments of Hong Kong. *Building and Environment* **2007**, *42*, 3669-3684. Available online: http://dx.doi.org/10.1016/j.buildenv.2006.09.011.

26. Giridharan R, Ganesan S,Lau SSY. Daytime urban heat island effect in high-rise and high-density residential developments in Hong Kong. *Energy and Buildings* **2004**, *36*, 525-534. Available online: http://dx.doi.org/10.1016/j.enbuild.2003.12.016.

Preprints (www.preprints.org) | NOT PEER-REVIEWED | Posted: 3 June 2019 doi:10.20944/preprints201906.0010.v1

Peer-reviewed version available at Sensors 2019, 19, 3459; doi:10.3390/s19163459

27. Jusuf SK,Wong NH. Development of empirical models for an estate level air temperature prediction in Singapore. Proceeding of Second International Conference on Countermeasures to Urban Heat Islands. University of California, Berkeley, 2009.

28. Jusuf SK, Ignatius M, Wong NH,Tan E, *STEVE Tool Plug-in for SketchUp: A User-Friendly Microclimatic Mapping Tool for Estate Development*, in *Sustainable Building and Built Environments to Mitigate Climate Change in the Tropics: Conceptual and Practical Approaches*, KARYONO TH, VALE R, VALE B, Editors. 2017, Springer International Publishing: Cham. p. 113-130.

29. He T, Liang S, Wang D, Cao Y, Gao F, Yu Y,Feng M. Evaluating land surface albedo estimation from Landsat MSS, TM, ETM +, and OLI data based on the unified direct estimation approach. *Remote Sensing of Environment* **2018**, *204*, 181-196. Available online: http://dx.doi.org/10.1016/j.rse.2017.10.031.

30. Valor E,Caselles V. Mapping land surface emissivity from NDVI: Application to European, African, and South American areas. *Remote Sensing of Environment* **1996**, *57*, 167-184. Available online: http://dx.doi.org/10.1016/0034-4257(96)00039-9.

31. Sobrino JA, Jimenez-Munoz JC, Soria G, Romaguera M, Guanter L, Moreno J, Plaza A,Martinez P. Land Surface Emissivity Retrieval From Different VNIR and TIR Sensors. *IEEE Trans. Geosci. Remote Sens.* **2008**, *46*, 316-327. Available online: http://dx.doi.org/10.1109/TGRS.2007.904834.

32. Gál T, Lindberg F,Unger J. Computing continuous sky view factors using 3D urban raster and vector databases: comparison and application to urban climate. *Theoretical and Applied Climatology* **2009**, *95*, 111-123. Available online: http://dx.doi.org/10.1007/s00704-007-0362-9.

33. Shi Y,Zhang Y. Remote sensing retrieval of urban land surface temperature in hot-humid region. *Urban Climate* **2018**, *24*, 299-310. Available online: http://dx.doi.org/10.1016/j.uclim.2017.01.001.

34. Liang S, Strahler AH,Walthall C. Retrieval of land surface albedo from satellite observations: A simulation study. *J. Appl. Meteor.* **1999**, *38*, 712-725. Available online: http://dx.doi.org/10.1175/1520-0450(1999)038<0712:ROLSAF>2.0.CO;2.

35. Shashua-Bar L,Hoffman ME. Quantitative evaluation of passive cooling of the UCL microclimate in hot regions in summer, case study: urban streets and courtyards with trees. *Building and Environment* **2004**, *39*, 1087-1099. Available online: http://dx.doi.org/10.1016/j.buildenv.2003.11.007.

36. Oke TR. Canyon geometry and the nocturnal urban heat island: Comparison of scale model and field observations. *Journal of Climatology* **1981**, *1*, 237-254. Available online: http://dx.doi.org/10.1002/joc.3370010304.

37. Watson ID,Johnson GT. Graphical estimation of sky view-factors in urban environments. *Journal of Climatology* **1987**, *7*, 193-197. Available online: http://dx.doi.org/10.1002/joc.3370070210.

38. Scarano M,Sobrino JA. On the relationship between the sky view factor and the land surface temperature derived by Landsat-8 images in Bari, Italy. *International Journal of Remote Sensing* **2015**, *36*, 4820-4835. Available online: http://dx.doi.org/10.1080/01431161.2015.1070325.

39. Scarano M,Mancini F. Assessing the relationship between sky view factor and land surface temperature to the spatial resolution. *International Journal of Remote Sensing* **2017**, *38*, 6910-6929. Available online: http://dx.doi.org/10.1080/01431161.2017.1368099.

40. Gillner S, Vogt J, Tharang A, Dettmann S,Roloff A. Role of street trees in mitigating effects of heat and drought at highly sealed urban sites. *Landscape and Urban Planning* **2015**, *143*, 33-42. Available online: http://dx.doi.org/https://doi.org/10.1016/j.landurbplan.2015.06.005.

Preprints (www.preprints.org) | NOT PEER-REVIEWED | Posted: 3 June 2019 doi:10.20944/preprints201906.0010.v1

Peer-reviewed version available at Sensors 2019, 19, 3459; doi:10.3390/s19163459

41. Lee H, Holst J,Mayer H. Modification of Human-Biometeorologically Significant Radiant Flux Densities by Shading as Local Method to Mitigate Heat Stress in Summer within Urban Street Canyons. *Advances in Meteorology* **2013**, *2013*, 13. Available online: http://dx.doi.org/10.1155/2013/312572.

42. Nakamura Y,Oke TR. Wind, temperature and stability conditions in an east-west oriented urban canyon. *Atmospheric Environment (1967)* **1988**, *22*, 2691-2700. Available online: http://dx.doi.org/10.1016/0004-6981(88)90437-4.

43. Bonafoni S,Keeratikasikorn C. Land Surface Temperature and Urban Density: Multiyear Modeling and Relationship Analysis Using MODIS and Landsat Data. **2018**, *10*, 1471. Available online: http://dx.doi.org/10.3390/rs10091471.

44. Jin M,Liang S. An Improved Land Surface Emissivity Parameter for Land Surface Models Using Global Remote Sensing Observations. *J. Climate* **2006**, *19*, 2867-2881. Available online: http://dx.doi.org/10.1175/jcli3720.1.

45. Baldridge AM, Hook SJ, Grove CI,Rivera G. The ASTER spectral library version 2.0. *Remote Sensing of Environment* **2009**, *113*, 711-715. Available online: http://dx.doi.org/10.1016/j.rse.2008.11.007.

46. Voogt JA,Oke TR. Complete urban surface temperatures. *J. Appl. Meteor.* **1997**, *36*, 1117-1132. Available online: http://dx.doi.org/10.1175/1520-0450(1997)036<1117:CUST>2.0.CO;2.

47. Grimmond CSB,Oke TR. Aerodynamic properties of urban areas derived from analysis of surface form. *J. Appl. Meteor.* **1999**, *38*, 1262-1292. Available online: http://dx.doi.org/10.1175/1520-0450(1999)038<1262:APOUAD>2.0.CO;2.

48. Gutman G,Ignatov A. The derivation of the green vegetation fraction from NOAA/AVHRR data for use in numerical weather prediction models. *International Journal of Remote Sensing* **1998**, *19*, 1533-1543. Available online: http://dx.doi.org/10.1080/014311698215333.

49. Zhang X, Liao C, Li J,Sun Q. Fractional vegetation cover estimation in arid and semi-arid environments using HJ-1 satellite hyperspectral data. *International Journal of Applied Earth Observation and Geoinformation* **2013**, *21*, 506-512. Available online: http://dx.doi.org/10.1016/j.jag.2012.07.003.

50. Jiménez-Muñoz JC, Sobrino JA, Plaza A, Guanter L, Moreno J,Martínez P. Comparison between fractional vegetation cover retrievals from vegetation indices and spectral mixture analysis: Case study of PROBA/CHRIS data over an agricultural area. *Sensors (Basel, Switzerland)* **2009**, *9*, 768-793. Available online: http://dx.doi.org/10.3390/s90200768.

51. Gál T,Unger J. A new software tool for SVF calculations using building and tree-crown databases. *Urban Climate* **2014**, *10*, 594-606. Available online: http://dx.doi.org/10.1016/j.uclim.2014.05.004.